

Customized optical chirality of vortex structured light through state and degree-of-polarization control

Kayn A. Forbes¹* and Dale Green¹

School of Chemistry, University of East Anglia, Norwich, Norfolk NR7 4TJ, United Kingdom



(Received 6 April 2023; accepted 18 May 2023; published 6 June 2023)

We show how both the ellipticity η and degree of polarization P influence the extraordinary optical chirality properties of nonparaxial vortex beams. We find that, in stark contrast to paraxial optics and nonvortex modes, extremely rich and tunable spatial distributions of optical chirality density can be produced by an optical vortex beam under tight focusing. We develop a theoretical description of how the optical chirality can be tailored for purpose by altering both the state η and degree of polarization P of the input vortex mode, along with the magnitude and sign of optical orbital angular momentum via the pseudoscalar topological charge ℓ . We expect that the results will have a significant role in both producing alternative techniques and improving existing methods in chiral nano-optics and structured light photonics.

DOI: [10.1103/PhysRevA.107.063504](https://doi.org/10.1103/PhysRevA.107.063504)

I. INTRODUCTION

Chiral objects are nonsuperimposable with their mirror image. Material chirality pervades the universe at all scales, from the spiraling arms of galaxies to our hands and feet, to the biomolecules responsible for life on earth. Light may also be chiral, most commonly manifest in circular polarization states, where the electromagnetic field vectors trace out helices that may twist to the left or right. This chirality associated with the handedness of polarization is often described in terms of the pseudoscalar optical helicity or chirality $\sigma = \pm 1$ where the upper (lower) sign refers to left-handed (right-handed). A prevalent method of studying material chirality is to use chiral light in chiroptical spectroscopy; classic examples include circular dichroism, optical rotation, and vibrational optical activities [1,2]. The basis of such spectroscopy is extremely simple: a right-handed (left-handed) molecule or nanostructure interacts with a left-handed circularly polarized photon $\sigma = 1$ in a different way than it does with a right-handed circularly polarized photon $\sigma = -1$, this discrimination is referred to as natural optical activity [1]. The importance of chiroptical spectroscopy cannot be overstated: essentially all the molecular building blocks of life (nucleosides, amino acids, proteins, carbohydrates, etc.) are chiral; over half of the developed pharmaceutical drugs are chiral [3], and considering the recent challenge faced globally by COVID-19 it is pertinent to state that chiral spectroscopy can be used to study viruses [4,5]. It is therefore easy to appreciate why chiroptical spectroscopy is a widespread and flourishing

area of research throughout science, being applied in chemical systems [1,5,6], biomolecules [7–10], and artificial nanostructures and metamaterials [11–16]. All these studies, while concerning an extremely diverse range of chiral materials, still predominantly rely on circularly polarized light as the chiral optical probe.

Structured light is a term which refers to the fact that, due to significant advances in optics technology, we can tailor beams of light to possess inhomogeneous polarization, amplitude, and phase, both spatially and temporally [8,9]. One of the most well-known types of structured light is the optical vortex, a generic term which denotes an electromagnetic field that possesses an azimuthal phase $\exp(i\ell\phi)$, where $\ell \in \mathbb{Z}$ is the pseudoscalar topological charge and ϕ is the azimuthal coordinate. Specific modes include Laguerre-Gaussian and Bessel beams. Optical vortices have found immense application in a diverse range of areas; see the latest reviews [17–24]. Optical vortices are chiral irrespective of their polarization: their helical wavefront (surface of constant phase) is chiral and can twist to the left, $\ell > 0$, or right, $\ell < 0$. Since 2018 there has been a surge in research activity applying the chirality of optical vortices in chiroptical light-matter interactions and spectroscopies [22,25]. Cutting-edge experiments include x-ray vortex dichroism of organometallic compounds [26], nonlinear vortex dichroism in chiral molecules as small as fenchone and limonene [27], and differential Raman scattering of vortex beams in liquid crystals [28].

Critical to engaging the chirality associated with the phase of an optical vortex is the consideration that it is a global property of the beam (its structure spans the transverse dimension of the beam, i.e., beam width), unlike polarization which is a local property. As such, in order for the chirality of materials to discriminate the handedness of the optical vortex, $\ell > 0$ or $\ell < 0$, the size scale must be relatively similar: for small chiral nanostructures and molecules the light must therefore be spatially confined, e.g., by tight focusing. It is well known that the state and degree of polarization of the

*k.forbes@uea.ac.uk

Published by the American Physical Society under the terms of the [Creative Commons Attribution 4.0 International license](https://creativecommons.org/licenses/by/4.0/). Further distribution of this work must maintain attribution to the author(s) and the published article's title, journal citation, and DOI.

input beam significantly influence the electromagnetic fields around the focal plane of a nonparaxial field [29,30]. All such previous studies looking at the optical chirality density of vortex beams have been concerned with beams that are fully polarized (i.e., degree of polarization P of the input beam before focusing is $P = 1$) and with the two extremes of ellipticity η , i.e., linearly polarized $\eta = 0$ or circularly polarized $\eta = \pm\pi/4$. In this study we look specifically at how the degree of polarization and ellipticity influences the optical chirality density of vortex beams in nano-optics. It is highlighted that varying these two experimentally controllable parameters produces an extremely rich and diverse number of landscapes of optical chirality density in vortex beams.

II. OPTICAL CHIRALITY DENSITY OF A NONPARAXIAL BESSEL BEAM

A. Electromagnetic fields of nonparaxial Bessel beams and optical chirality density

We use analytical theory to describe nonparaxial Bessel beams. We use the standard language first introduced by Lax *et al.* [31]. The zeroth-order transverse electromagnetic fields

T_0 for a Bessel beam propagating along z are

$$\begin{aligned} \mathbf{E}^{(T_0)} &= (\alpha\hat{x} + \beta\hat{y})J_\ell[k_t r]E_0 e^{i(k_z z + \ell\phi - \omega t)}, \\ \mathbf{B}^{(T_0)} &= (\alpha\hat{y} - \beta\hat{x})\frac{k_z}{k}J_\ell[k_t r]B_0 e^{i(k_z z + \ell\phi - \omega t)}, \end{aligned} \quad (1)$$

where (α, β) are the generalized Jones vectors; E_0 is the electric field amplitude; $B_0 = E_0/c$; $k^2 = \omega^2/c^2 = k_x^2 + k_y^2 + k_z^2 = k_t^2 + k_z^2$ is the square of the wave number, with $k_z = \sqrt{k^2 - k_t^2}$ and $k_t = \sqrt{k_x^2 + k_y^2}$; $J_\ell[k_t r]$ are Bessel functions of the first kind; $\exp(i\ell\phi)$ is the azimuthal phase mentioned in the Introduction; and ω is the mean circular frequency. We drop the dependences $[\dots]$ from now on for notational brevity. Both fields in (1) describe a paraxial mode and the electromagnetic fields of a Bessel beam correctly when $k \approx k_z$, e.g., a well-collimated beam. However, it is easy to show that (1) do not satisfy Maxwell's equations in their current form, e.g., $\nabla \cdot \mathbf{E}^{(T_0)} \neq 0$. By using Maxwell's equations in a well-known method first developed by Lax *et al.* [31], we can generate the electromagnetic fields of a Bessel beam up to second order in a smallness parameter (k_t/k_z), and thus they now include the zeroth-order transverse field T_0 ; the first-order longitudinal field L_1 (polarized along \hat{z}); and the second-order transverse fields T_2 (see Supplemental Material [32] for derivation):

$$\mathbf{E} = \begin{bmatrix} (\alpha\hat{x} + \beta\hat{y})J_\ell + \hat{z}\frac{ik_t}{2k_z}(\{\alpha + i\beta\}e^{-i\phi}J_{\ell-1} + \{i\beta - \alpha\}e^{i\phi}J_{\ell+1}) \\ + \frac{k_t^2}{4k^2}(\hat{x}[2\alpha J_\ell + J_{\ell-2}\{\alpha + i\beta\}e^{-2i\phi} + J_{\ell+2}\{\alpha - i\beta\}e^{2i\phi}] \\ + \hat{y}[2\beta J_\ell + J_{\ell-2}\{i\alpha - \beta\}e^{-2i\phi} + J_{\ell+2}\{-\beta - i\alpha\}e^{2i\phi}]) \end{bmatrix} E_0 e^{i(k_z z + \ell\phi - \omega t)}, \quad (2)$$

$$\mathbf{B} = \begin{bmatrix} (\alpha\hat{y} - \beta\hat{x})\frac{k_z}{k}J_\ell + \hat{z}\frac{ik_t}{2k}(\{i\alpha - \beta\}e^{-i\phi}J_{\ell-1} + \{i\alpha + \beta\}e^{i\phi}J_{\ell+1}) \\ + \frac{k_t^2}{4kk_z}(\hat{x}[-2\beta J_\ell + J_{\ell-2}\{i\alpha - \beta\}e^{-2i\phi} + J_{\ell+2}\{-i\alpha - \beta\}e^{2i\phi}] \\ + \hat{y}[2\alpha J_\ell + J_{\ell-2}\{-i\beta - \alpha\}e^{-2i\phi} + J_{\ell+2}\{i\beta - \alpha\}e^{2i\phi}]) \end{bmatrix} B_0 e^{i(k_z z + \ell\phi - \omega t)}. \quad (3)$$

Both (2) and (3) can accurately describe a paraxial or nonparaxial (e.g., tightly focused) Bessel beam. The smallness parameter for a Bessel beam is k_t/k_z : increasing the size of this factor essentially accounts for tightly focusing the beam. For example, in the far field $k_t/k_z \approx 0$ (or $k \approx k_z$) for a z -propagating beam and the field can essentially be described by the zeroth-order transverse fields in (2) and (3), or equally (1) to an almost exact approximation (i.e., a paraxial description) [33]. By focusing the beam k_t/k_z becomes larger and the additional longitudinal and transverse terms in (2) and (3) become important in magnitude and are responsible for the extraordinary properties of structured light in nano-optics [34–36]. Thus, the paraxial description (1) no longer suffices under tight focusing. Throughout this paper we refer to the polarization properties of the input light in the far field as two-dimensional (2D), i.e., the zeroth-order electric field polarization state. The polarization properties of the nonparaxial field under spatial confinement are generally referred to as three-dimensional (3D) polarization [37–39].

The optical chirality density C for a quasimonochromatic beam may be defined as (see Supplemental Material [32] for

further information) [40–42]

$$C = -\frac{\varepsilon_0\omega}{2}\text{Im}(\bar{\mathbf{E}} \cdot \mathbf{B}), \quad (4)$$

where the overbar denotes complex conjugation. Crudely put, this dynamic property of light (conserved in free space) gives a measure of how chiral the optical field is. It is related to the optical helicity; interested readers are referred to Refs. [40,42] for further information. Chiral light-matter interactions are produced from multipolar interferences that give space-odd, time-even tensors for the material [1,43]. It is of utmost importance to appreciate that (4) couples to the electric dipole magnetic dipole (E1M1) interferences supported only by chiral materials. The interaction of light and matter leads to a transition amplitude consisting of a sum of multipolar couplings: electric dipole E1 + magnetic dipole M1 + electric quadrupole E2 and so on [1,44]. The transition probability of any given optical process (absorption, scattering, etc.) depends on the square of this amplitude. While the ensuing E1E1 and M1M1 terms are independent of both material and optical chirality (being space even and time even), the E1M1 cross terms mix the electric and magnetic dipole interactions,

leading to chiral observables directly proportional to (4). The optical chirality, defined by (4), therefore does not account for all chiral light-matter interactions, for example, those which stem from electric dipole electric quadrupole interferences (E1E2). Inserting (2) and (3) into (4) gives the optical chirality density as (full systematic derivation in Supplemental Material [32])

$$C = -\frac{I\omega}{c^2} \left[\frac{k_z}{k} J_\ell^2 P \sin 2\eta + \frac{k_t^2}{4kk_z} \left(2 \left\{ 1 + \frac{k_z^2}{k^2} \right\} J_\ell^2 P \sin 2\eta + \{P \sin 2\eta + 1\} J_{\ell-1}^2 + \{P \sin 2\eta - 1\} J_{\ell+1}^2 \right) + \left(\frac{k_t^4}{8k^3 k_z} \right) (2J_\ell^2 P \sin 2\eta + J_{\ell-2}^2 \{P \sin 2\eta + 1\} + J_{\ell+2}^2 \{P \sin 2\eta - 1\}) \right], \quad (5)$$

where $I = c\varepsilon_0 E_0^2/2$ is the intensity of the beam; P is the 2D degree of polarization of the input, which takes values between 0 for unpolarized light and 1 for polarized light, i.e., $0 \leq P \leq 1$, and is formally defined as the ratio of the intensity of the polarized part of the beam to the total intensity [45]; η defines the degree of 2D polarization ellipticity and is formally defined as the ratio of the minor (b) and major (a) axes of the polarization ellipse $\tan \eta = b/a$: $\eta = 0$ is linearly polarized light; $\eta = \pm\pi/4$ is pure circular; and $-\pi/4 < \eta < \pi/4$ corresponds to elliptically polarized light (positive signed is right handed, negative sign left handed). The first term in square brackets in (5) corresponds to the well-known optical chirality density for a paraxial beam of light which stems purely from a degree of ellipticity in the 2D polarization state, proportional to the third Stokes parameter, and clearly requires $P \neq 0$. All the other terms correspond to the optical chirality density generated by first-order longitudinal and second-order transverse fields which become important under the nonparaxial conditions we are interested in. Note that no terms in (5) depend on the azimuth θ , i.e., the orientation of the 2D polarization ellipse.

B. Optical chirality density of a Bessel beam with pure $P = 1$ 2D polarization

The optical chirality density (5) is plotted in Figs. 1 and 2 for $P = 1$ and $k_t/k_z = 0.6315$ (i.e., tightly focused).

The leftmost column in Figs. 1 and 2 corresponds to an input 2D linearly polarized ($\eta = 0$) Bessel beam; the rightmost column corresponds to a circularly polarized Bessel beam, and in between shows varying degrees of ellipticity. First, we note that 2D linearly polarized vortex beams under tight focusing exhibit nonzero optical chirality densities [46,47]: this is in stark contrast to plane waves or paraxial beams, where there must be a degree of ellipticity η in the polarization state. Furthermore, comparing Figures 1 and 2 shows that the optical chirality density spatial distributions reverse depending on the sign of ℓ , i.e., the vortex wavefront handedness. It is this nonzero chirality associated with tightly focused linearly polarized vortex beams which is responsible for vortex dichroism [26,48] and vortex differential scattering [49]: chiral materials absorb and scatter linearly polarized nonparaxial vortex beams at different rates depending on whether the input beam is $\ell > 0$ or $\ell < 0$.

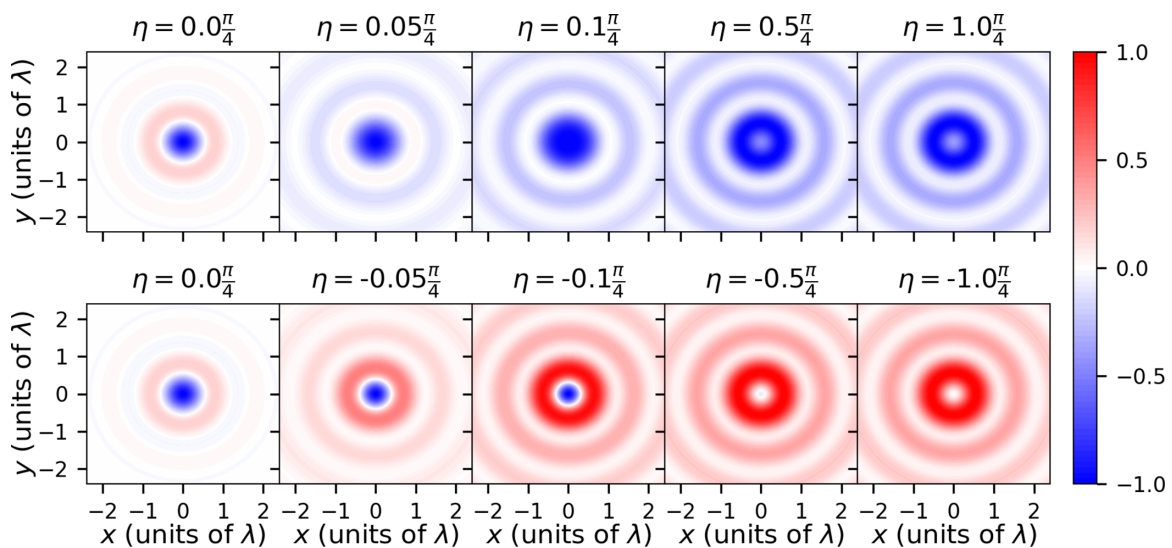


FIG. 1. Evolution of the optical chirality density of an $\ell = 1$ Bessel beam in the focal plane with varying 2D-polarization ellipticity η . The input polarization progresses from linearly polarized $\eta = 0$ through varying degrees of ellipticity $-\pi/4 < \eta < \pi/4$ until it reaches pure circular polarization $\eta = \pm\pi/4$. The top row cycles through right-handed polarization, the bottom row left-handed polarization. In all plots $k_t/k_z = 0.6315$, $\lambda = 729$ nm, and each plot is normalized individually.

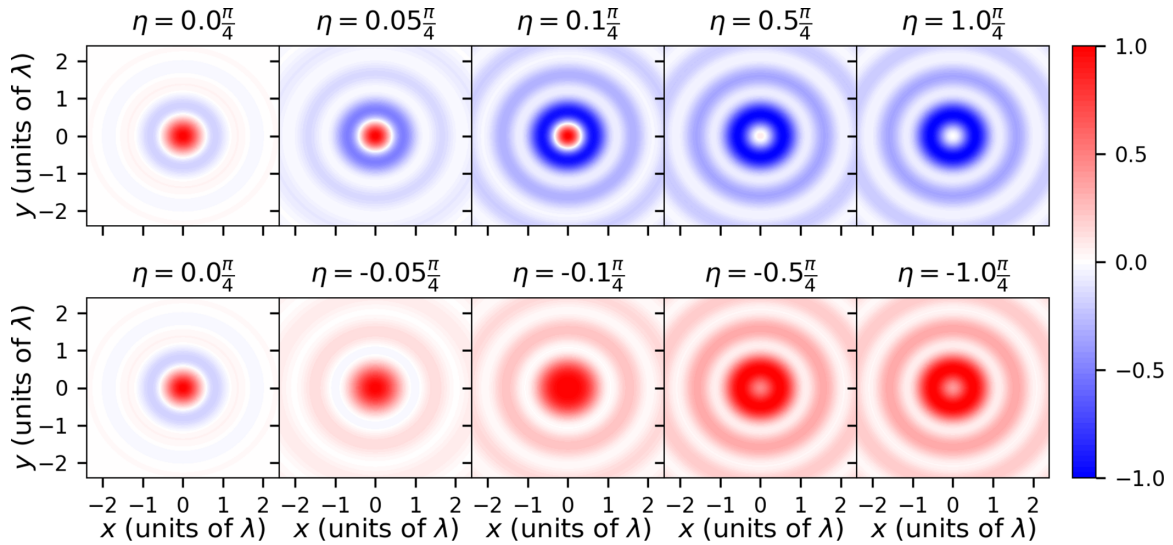


FIG. 2. Evolution of the optical chirality density of an $\ell = -1$ Bessel beam in the focal plane with varying 2D-polarization ellipticity η . (Everything else is the same as Fig. 1.)

Moving across the rows in Figs. 1 and 2 we are changing the state of 2D polarization by increasing the degree of 2D ellipticity of the input and this significantly alters the spatial distribution of optical chirality density. It is noticeable that we soon lose half of the rings of chirality density (the left-hand panels have five rings, for example, whereas the rightmost have three). We also note that there is a chiral interplay between the signs of ℓ (vortex handedness) and the sign of η (polarization handedness): this is due to spin-orbit interactions of light. Most striking is the fact that when the handednesses of the vortex and polarization are opposite (e.g., left-handed vortex, right-handed ellipticity) we produce on-axis optical chirality densities of the same sign as the ellipticity handedness; where they are of the same handedness there is an opposite signed chirality density which progresses to a null density along the axis. This is somewhat similar to the be-

havior of the intensity of tightly focused vortex beams, where it is often described in terms of parallel and antiparallel spin and orbital angular momentum of the beams [35,50] (also see Appendix B). Furthermore, in the cases of $\eta \approx \pm\pi/40$, $\ell \pm 1$ (i.e., we have antiparallel polarization and vortex handedness) we produce the spatial distribution of the optical chirality of an $\ell = 0$ mode (see Fig. 3, for example), even though $\ell \neq 0$.

It is simple to highlight the significant influence orbital angular momentum of light (OAM) and vortex chirality have on optical chirality by plotting (5) for $\ell = 0$, i.e., a tightly focused nonvortex beam with no OAM. Figure 3 highlights that when there is no degree of ellipticity in the 2D polarization state ($\eta = 0$) the optical chirality is zero, and while the magnitude of the optical chirality density increases with increasing ellipticity, the spatial distributions are invariant to both magnitude and sign (handedness). This is clearly in stark

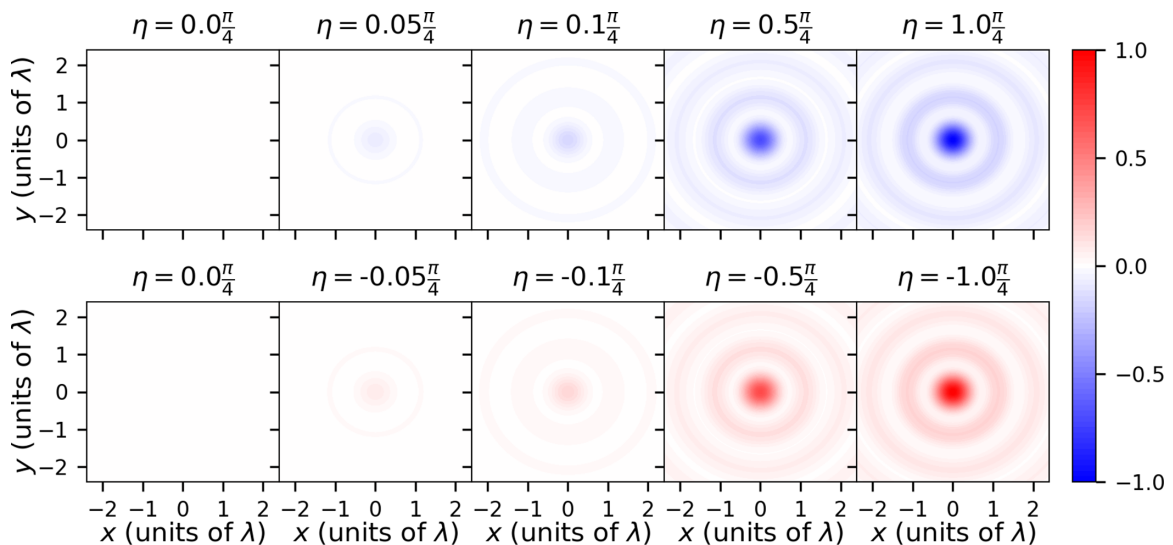


FIG. 3. Evolution of the optical chirality density of a tightly focused $\ell = 0$ Bessel beam in the focal plane with varying 2D-polarization ellipticity η . Each plot is normalized against $|\eta| = \pi/4$ plots. (Everything else is the same as Fig. 1.)

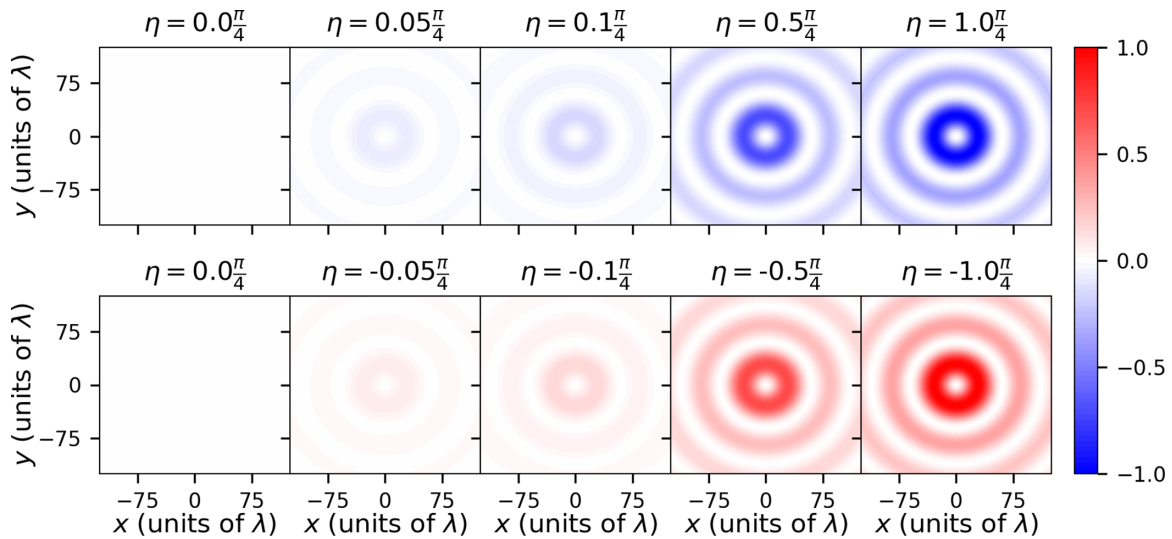


FIG. 4. Evolution of the optical chirality density of an $\ell = 1$ and $\ell = -1$ weakly focused $(k_t/k_z) = 0.01$ Bessel beam in the focal plane with varying 2D-polarization ellipticity η . Each plot is normalized against $|\eta| = \pi/4$ plots. (Everything else is the same as Fig. 1.)

contrast to tightly focused $\ell \neq 0$ Bessel modes which possess OAM in Figs. 1 and 2.

Another degree of freedom we can control is the magnitude of ℓ for the input beam, and plots for $\ell = \pm 2$ modes can be found in Appendix A. The optical chirality spatial distributions follow a pattern similar to Figs. 1 and 2 for the larger value of ℓ , the main difference being the increase in ring widths analogous to the behavior of the intensity of vortex beams.

In order to appreciate the role tight focusing has in producing the extraordinary optical chirality properties highlighted in Figs. 1 and 2 it is useful to plot (5) under paraxial conditions. We gave a qualitative physical reason for the necessity for tight focusing in the Introduction: here we see it played out by the mathematics. The analogous plots of Figs. 1 and 2 for a weakly focused $(k_t/k_z) = 0.01$, essentially a paraxial beam, can be found in Fig. 4, where it is readily observed that all

the extraordinary properties of the nonparaxial field are lost. Indeed, there are no observable spin-orbit interactions; there is a vanishingly small (practically zero) chirality for linearly polarized inputs $\eta = 0$, and the optical chirality density does not depend on the sign of vortex handedness: the plots in Fig. 4 are identical for $\ell = \pm 1$.

C. Optical chirality density of a Bessel beam with partial 2D polarization

Between the two extremes of completely polarized light $P = 1$ and unpolarized light $P = 0$ we have partially polarized light. In the previous section we studied how the state of polarization (specifically the degree of ellipticity η) affects the optical chirality density in the focal plane for a fully polarized beam $P = 1$; in this section we will study how the degree of polarization P affects the optical chirality density for a set of

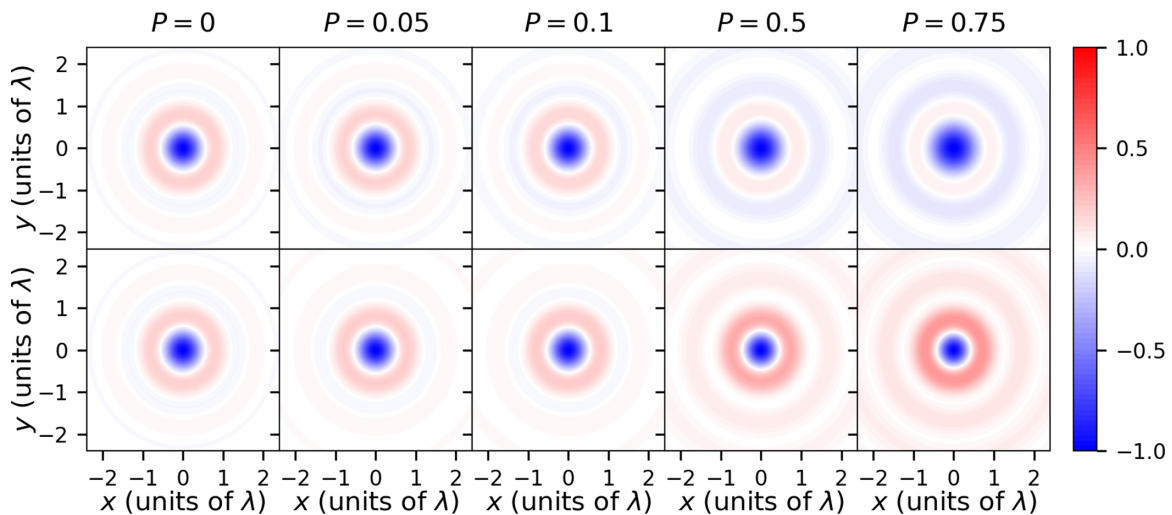


FIG. 5. Evolution of the optical chirality density of an $\ell = 1$ Bessel beam in the focal plane with varying degree of polarization P of an elliptically polarized beam $\eta = \pm\pi/80$. The top row cycles through right-handed polarization $\eta = \pi/80$, the bottom row left-handed polarization $\eta = -\pi/80$. In all plots $k_t/k_z = 0.6315$, $\lambda = 729$ nm, and each plot is normalized individually.

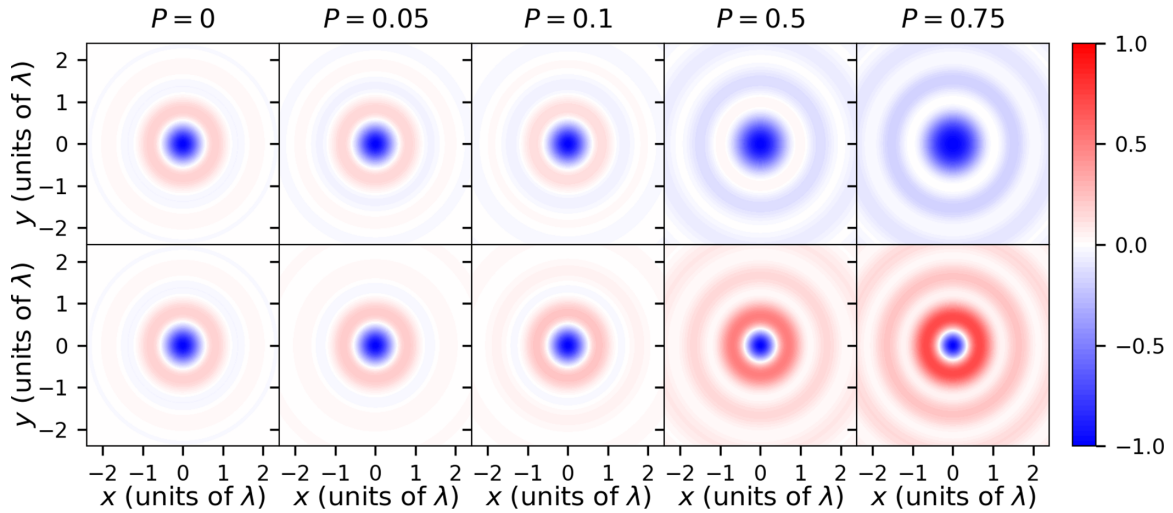


FIG. 6. Evolution of the optical chirality density of an $\ell = 1$ Bessel beam in the focal plane with varying degree of polarization P of an elliptically polarized beam $\eta = \pm\pi/40$. Everything else is as in Fig. 5.

fixed polarization states: Fig. 5: $\eta = \pi/80$; Fig. 6: $\eta = \pi/40$; and Fig. 7: $\eta = \pi/8$.

First we must point out the remarkable result that even when the beam is unpolarized $P = 0$ (leftmost columns in Figs. 5–7), the optical chirality density is nonzero [51]. In other words, we can get chiral light-matter interactions and do chiral spectroscopy with unpolarized sources of light [51–53]. Furthermore, Figs. 5–7 clearly highlight how increasing (or decreasing) the degree of 2D polarization P significantly influences the spatial distribution of the optical chirality density, even though the state of 2D polarization η for the polarized part of the field is fixed in each case (and so too is the value of ℓ).

Another way to gauge the influence of P is to compare how the spatial distribution of the optical chirality of a fully 2D polarized beam for a given η (from Figs. 1 and 2) compares to that where $P \neq 1$ (Figs. 5–7). As an example, Fig. 7 shows the optical chirality density of a partially polarized beam with

$\eta = \pi/8$, which can be compared to the fourth column in Fig. 1. We see that Fig. 7 shows that a $P = 0.1$, $\eta = \pi/8$ beam gives a similar optical chirality density as a $P = 1$, $\eta = \pi/80$ beam. In this section we have concentrated on $\ell = 1$ modes; however, the corresponding $\ell = -1$ plots can be found in the Supplemental Material [32], alongside the $\ell = \pm 2$ mode plots.

III. DISCUSSION AND CONCLUSION

Here we have systematically studied how the 2D state and degree of polarization of an input paraxial vortex beam influences the optical chirality density of the nonparaxial field around the focal plane. We have highlighted the extremely rich spatial distributions of optical chirality density that can be produced by optical vortex beams in nano-optics. This optical chirality density can be tailored for purpose by altering both the state and degree of 2D polarization of the

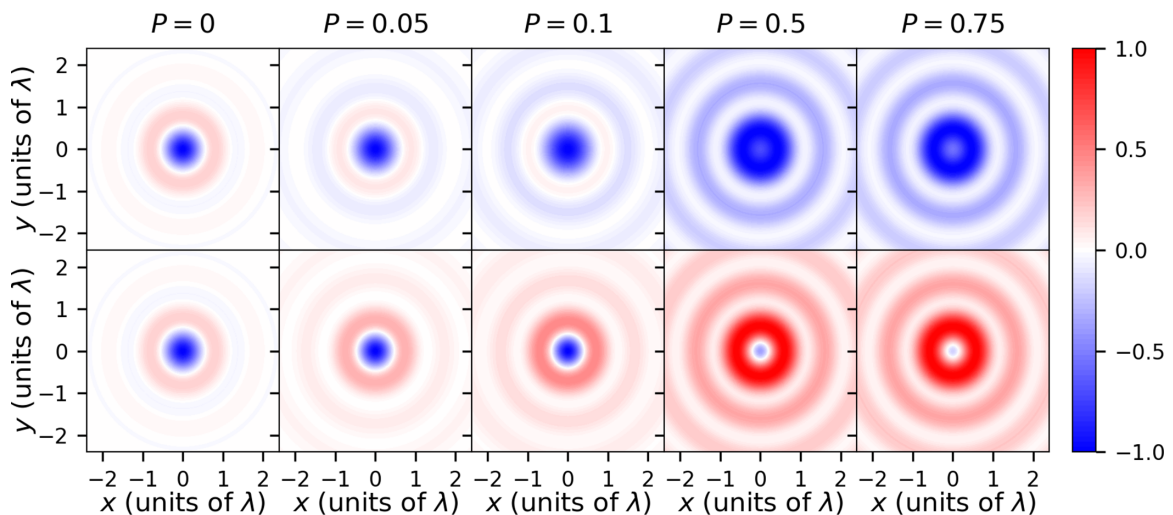


FIG. 7. Evolution of the optical chirality density of an $\ell = 1$ Bessel beam in the focal plane with varying degree of polarization P of an elliptically polarized beam $\eta = \pm\pi/8$. Everything else is as in Fig. 5.

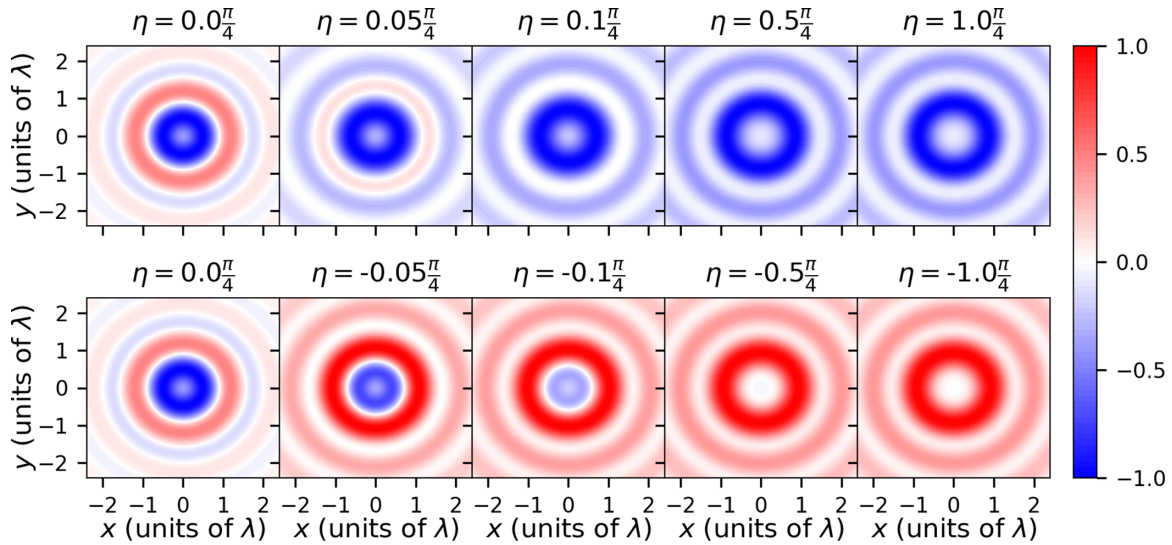


FIG. 8. Evolution of the optical chirality density of an $\ell = 2$ Bessel beam in the focal plane with varying 2D-polarization ellipticity η . The input polarization progresses from linearly polarized $\eta = 0$ through varying degrees of ellipticity $-\pi/4 < \eta < \pi/4$ until it reaches pure circular polarization $\eta = \pm\pi/4$. The top row cycles through right-handed polarization, the bottom row left-handed polarization. In all plots $k_r/k_z = 0.6315$, $\lambda = 729$ nm, and each plot is normalized individually.

input vortex mode, along with the magnitude and sign of OAM through ℓ . It must be remembered that the optical chirality density produced by paraxial beams or plane waves requires both $P \neq 0$ and $\eta \neq 0$, and altering these parameters does not lead to any observable variations in the spatial distributions of the optical chirality density; they just vary in magnitude (e.g., Fig. 4). Comparison between this currently prevalent optical probe in chiroptical spectroscopy versus the optical chirality of nonparaxial vortex beams we have highlighted in this work makes it readily clear why structured light chirality is poised to revolutionize chiral light-matter interactions [22,25,54].

It is worth briefly discussing another extraordinary property of optical fields in nano-optics at this juncture: the transverse spin momentum of light [34,55]. There have been

a number of recent studies looking at the influence of the state and degree of 2D polarization on this property [56–59]. Like the optical chirality density of optical vortex beams, the transverse spin momentum density of light occurs even if the optical source is 2D unpolarized [56,57]. This property of transverse spin is extremely generic for confined electromagnetic fields, being present in surface evanescent waves and tightly focused laser beams, for example. However, the optical chirality density which exists for 2D unpolarized light strictly only occurs in optical vortex beams [51]. It is rather interesting to reflect on the extraordinary fact that light can possess both spin angular momentum and optical chirality density for 2D unpolarized fields, and that the state and degree of 2D polarization significantly influence the spatial distributions of these quantities.

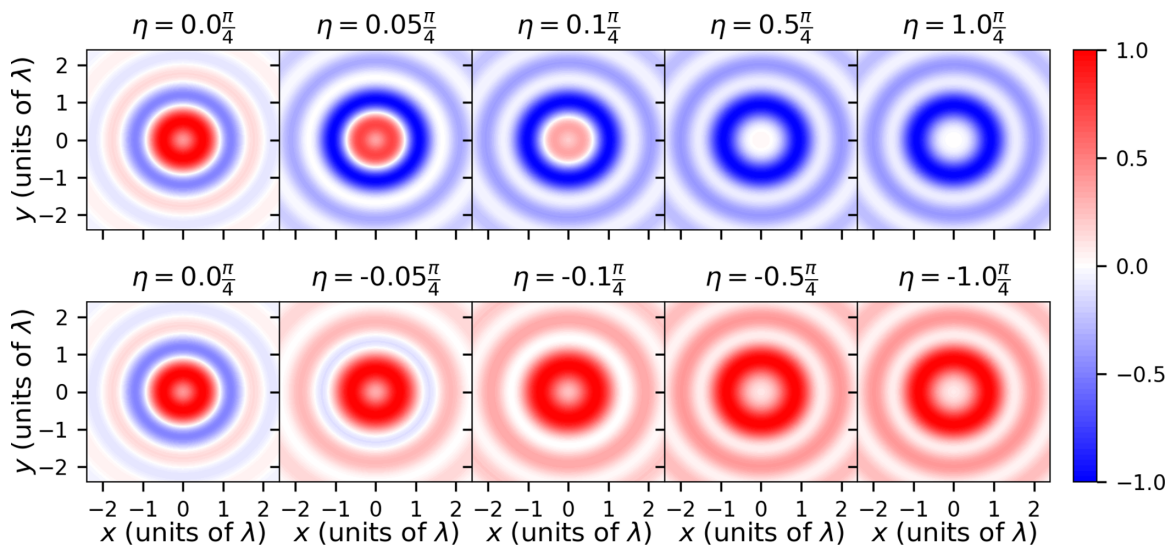


FIG. 9. Evolution of the optical chirality density of an $\ell = -2$ Bessel beam in the focal plane with varying 2D-polarization ellipticity η . (Everything else is the same as Fig. 8.)

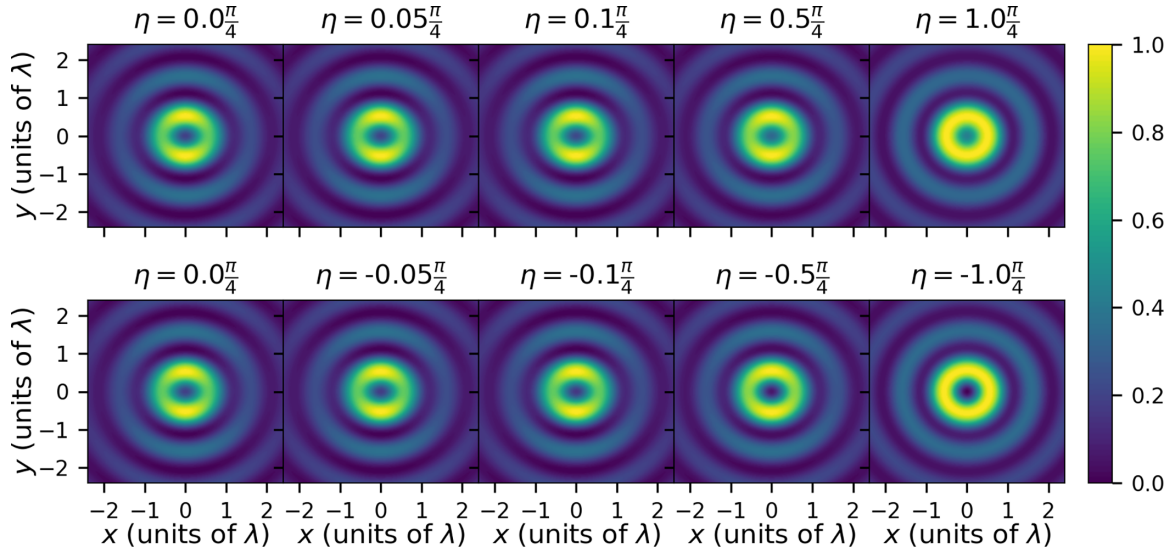


FIG. 10. Evolution of the intensity of an $\ell = 1$ Bessel beam in the focal plane with varying 2D-polarization ellipticity η . The input polarization progresses from linearly polarized $\eta = 0$ through varying degrees of ellipticity $-\pi/4 < \eta < \pi/4$ until it reaches pure circular polarization $\eta = \pm\pi/4$. The orientation of the 2D-polarization ellipse is zero. The top row cycles through right-handed polarization, the bottom row left-handed polarization. In all plots $k_t/k_z = 0.6315$, $\lambda = 729$ nm, and each plot is normalized individually.

As previously mentioned in the Introduction, to date practically all chiroptical spectroscopy and chiral light-matter interactions have utilized circularly polarized light (e.g., unstructured Gaussian beams) as the chiral optical probe. The optical chirality density for vortex beams we have studied has already been proven to offer significant advancements in both generating novel and improving existing applications in chiral nano-optics [25–28,52]. Here we have shown that this extraordinary optical chirality of structured light is able to be tailored for purpose. Future studies are aimed towards other forms of structured light which have enhanced chiral properties [60], such as vector vortex modes, alongside the influence of second-order coherence.

APPENDIX A: ADDITIONAL CHIRALITY DENSITY DISTRIBUTIONS FOR PURELY POLARIZED LIGHT $P = 1$

Here we provide additional plots of the spatial distribution for purely polarized Bessel beams relevant to Sec. II A of the main text. Figures 8 and 9 show the spatial distribution of the optical chirality density equation (6) from the main text for cases of $|\ell| = 2$, i.e., showing the effects of increasing the OAM of the input beam.

APPENDIX B: ENERGY DENSITY DISTRIBUTIONS OF NONPARAXIAL BESSEL BEAMS

The corresponding time-averaged electric energy densities $w_E = \frac{\epsilon_0}{2} \text{Re}(\vec{E} \cdot \vec{E})$, proportional to the intensity, for Bessel

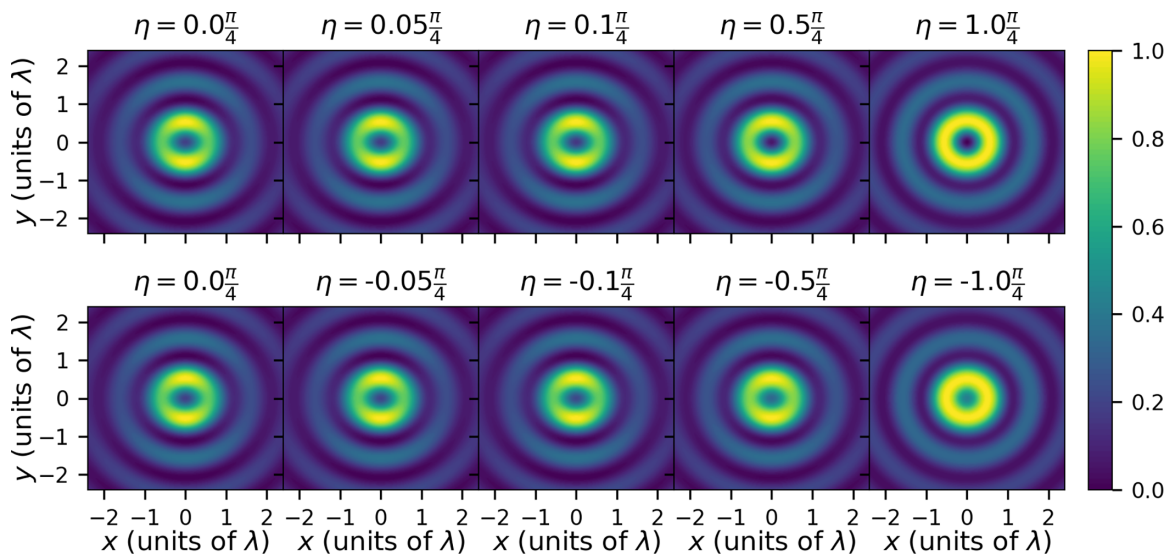


FIG. 11. Evolution of the intensity of an $\ell = -1$ Bessel beam in the focal plane with varying 2D-polarization ellipticity η . (Everything else is the same as Fig. 10.)

beams under the identical conditions as Figs. 1 and 2 of the main text are provided here. Unlike the optical chirality density (5), displayed in Figs. 1 and 2, the energy density (intensity) for nonparaxial beams is dependent on

the orientation of the 2D polarization ellipse, i.e., the azimuthal angle θ . In Figs. 10 and 11 we choose $\theta = 0$, such that for the case of $\eta = 0$ the 2D state of polarization is x polarized.

-
- [1] L. D. Barron, *Molecular Light Scattering and Optical Activity* (Cambridge University Press, Cambridge, 2009).
- [2] P. L. Polavarapu, *Chiroptical Spectroscopy: Fundamentals and Applications* (CRC Press, Boca Raton, FL, 2016).
- [3] L. A. Nguyen, H. He, and C. Pham-Huy, Chiral drugs: An overview, *Int. J. Biomed. Sci.* **2**, 85 (2006).
- [4] T. Kakkar, C. Keijzer, M. Rodier, T. Bukharova, M. Taliansky, A. J. Love, J. J. Milner, A. S. Karimullah, L. D. Barron, N. Gadegaard, A. J. Laphorn, and M. Kadodwala, Superchiral near fields detect virus structure, *Light Sci. Appl.* **9**, 195 (2020).
- [5] M. Krupová, J. Kessler, and P. Bouř, Recent trends in chiroptical spectroscopy: Theory and applications of vibrational circular dichroism and Raman optical activity, *ChemPlusChem* **85**, 561 (2020).
- [6] D. Leung, S. O. Kang, and E. V. Anslyn, Rapid determination of enantiomeric excess: A focus on optical approaches, *Chem. Soc. Rev.* **41**, 448 (2012).
- [7] J. Kumar, H. Eraña, E. López-Martínez, N. Claes, V. F. Martín, D. M. Solís, S. Bals, A. L. Cortajarena, J. Castilla, and L. M. Liz-Marzán, Detection of amyloid fibrils in Parkinson's disease using plasmonic chirality, *Proc. Natl. Acad. Sci. USA* **115**, 3225 (2018).
- [8] N. Berova, P. L. Polavarapu, K. Nakanishi, and R. W. Woody, *Comprehensive Chiroptical Spectroscopy, Volume 2: Applications in Stereochemical Analysis of Synthetic Compounds, Natural Products, and Biomolecules* (John Wiley & Sons, Inc., Hoboken, NJ, 2012).
- [9] L. D. Barron, The development of biomolecular Raman optical activity spectroscopy, *Biomed. Spectrosc. Imaging* **4**, 223 (2015).
- [10] O. Ávalos-Ovando, E. Y. Santiago, A. Movsesyan, X.-T. Kong, P. Yu, L. V. Besteiro, L. K. Khorashad, H. Okamoto, J. M. Slocik, and M. A. Correa-Duarte, Chiral bioinspired plasmonics: A paradigm shift for optical activity and photochemistry, *ACS Photonics* **9**, 2219 (2022).
- [11] E. S. Goerlitzer, A. S. Puri, J. J. Moses, L. V. Poulikakos, and N. Vogel, The beginner's guide to chiral plasmonics: Mostly harmless theory and the design of large-area substrates, *Adv. Opt. Mater.* **9**, 2100378 (2021).
- [12] L. Ohnoutek, J.-Y. Kim, J. Lu, B. J. Olohan, D. M. Răsădean, G. D. Pantoş, N. A. Kotov, and V. K. Valev, Third-harmonic Mie scattering from semiconductor nanohelices, *Nat. Photonics* **16**, 126 (2022).
- [13] A. Kakkanattu, N. Eerqing, S. Ghamari, and F. Vollmer, Review of optical sensing and manipulation of chiral molecules and nanostructures with the focus on plasmonic enhancements [Invited], *Opt. Express* **29**, 12543 (2021).
- [14] Y. Chen, W. Du, Q. Zhang, O. Ávalos-Ovando, J. Wu, Q.-H. Xu, N. Liu, H. Okamoto, A. O. Govorov, and Q. Xiong, Multidimensional nanoscopic chiroptics, *Nat. Rev. Phys.* **4**, 113 (2022).
- [15] L. A. Warning, A. R. Miandashti, L. A. McCarthy, Q. Zhang, C. F. Landes, and S. Link, Nanophotonic approaches for chirality sensing, *ACS Nano* **15**, 15538 (2021).
- [16] X.-T. Kong, L. V. Besteiro, Z. Wang, and A. O. Govorov, Plasmonic chirality and circular dichroism in bioassembled and nonbiological systems: Theoretical background and recent progress, *Adv. Mater.* **32**, 1801790 (2020).
- [17] A. Forbes, M. de Oliveira, and M. R. Dennis, Structured light, *Nat. Photonics* **15**, 253 (2021).
- [18] A. Forbes, Structured light from lasers, *Laser Photonics Rev.* **13**, 1900140 (2019).
- [19] Y. Shen, X. Wang, Z. Xie, C. Min, X. Fu, Q. Liu, M. Gong, and X. Yuan, Optical vortices 30 years on: OAM manipulation from topological charge to multiple singularities, *Light Sci. Appl.* **8**, 90 (2019).
- [20] Y. Yang, Y. Ren, M. Chen, Y. Arita, and C. Rosales-Guzmán, Optical trapping with structured light: A review, *Adv. Photonics* **3**, 034001 (2021).
- [21] C. Rosales-Guzmán, B. Ndagano, and A. Forbes, A review of complex vector light fields and their applications, *J. Opt.* **20**, 123001 (2018).
- [22] A. Porfirev, S. Khonina, and A. Kuchmizhak, Light-matter interaction empowered by orbital angular momentum: Control of matter at the micro- and nanoscale, *Prog. Quantum Electron.* **88**, 100459 (2023).
- [23] M. Babiker, D. L. Andrews, and V. E. Lembessis, Atoms in complex twisted light, *J. Opt.* **21**, 013001 (2018).
- [24] H. Yang, Z. Xie, H. He, Q. Zhang, and X. Yuan, A perspective on twisted light from on-chip devices, *APL Photonics* **6**, 110901 (2021).
- [25] K. A. Forbes and D. L. Andrews, Orbital angular momentum of twisted light: Chirality and optical activity, *J. Phys. Photonics* **3**, 022007 (2021).
- [26] J. R. Rouxel, B. Rösner, D. Karpov, C. Bacellar, G. F. Mancini, F. Zinna, D. Kinschel, O. Cannelli, M. Oppermann, and C. Svetina, Hard x-ray helical dichroism of disordered molecular media, *Nat. Photonics* **16**, 570 (2022).
- [27] J.-L. Bégin, A. Jain, A. Parks, F. Hufnagel, P. Corkum, E. Karimi, T. Brabec, and R. Bhardwaj, Nonlinear helical dichroism in chiral and achiral molecules, *Nat. Photonics* **17**, 82 (2023).
- [28] S. Müllner, F. Büscher, A. Möller, and P. Lemmens, Discrimination of Chiral and Helical Contributions to Raman Scattering of Liquid Crystals Using Vortex Beams, *Phys. Rev. Lett.* **129**, 207801 (2022).
- [29] M. Chekhova and P. Banzer, Polarization of light, in *Classical, Quantum, and Nonlinear Optics* (Walter de Gruyter GmbH & Co KG, Berlin, 2021).
- [30] L. Novotny and B. Hecht, *Principles of Nano-Optics* (Cambridge University Press, Cambridge, 2012).

- [31] M. Lax, W. H. Louisell, and W. B. McKnight, From Maxwell to paraxial wave optics, *Phys. Rev. A* **11**, 1365 (1975).
- [32] See Supplemental Material at <http://link.aps.org/supplemental/10.1103/PhysRevA.107.063504> for a complete derivation of the optical chirality density and additional plots of the chirality density distributions for partially polarized light.
- [33] K. A. Forbes, D. Green, and G. A. Jones, Relevance of longitudinal fields of paraxial optical vortices, *J. Opt.* **23**, 075401 (2021).
- [34] A. Aiello, P. Banzer, M. Neugebauer, and G. Leuchs, From transverse angular momentum to photonic wheels, *Nat. Photonics* **9**, 789 (2015).
- [35] K. Y. Bliokh, M. A. Alonso, E. A. Ostrovskaya, and A. Aiello, Angular momenta and spin-orbit interaction of nonparaxial light in free space, *Phys. Rev. A* **82**, 063825 (2010).
- [36] K. Y. Bliokh, A. Aiello, and M. A. Alonso, Spin-orbit interactions of light in isotropic media, in *The Angular Momentum of Light* (Cambridge University Press, Cambridge, 2012), pp. 174–245.
- [37] M. A. Alonso, Geometric descriptions for the polarization for nonparaxial optical fields: A tutorial, *Adv. Opt. Photonics* **15**, 176 (2023).
- [38] C. J. R. Sheppard, Jones and Stokes parameters for polarization in three dimensions, *Phys. Rev. A* **90**, 023809 (2014).
- [39] K. Lindfors, A. Priimagi, T. Setälä, A. Shevchenko, A. T. Friberg, and M. Kaivola, Local polarization of tightly focused unpolarized light, *Nat. Photonics* **1**, 228 (2007).
- [40] R. P. Cameron, S. M. Barnett, and A. M. Yao, Optical helicity, optical spin and related quantities in electromagnetic theory, *New J. Phys.* **14**, 053050 (2012).
- [41] K. Y. Bliokh and F. Nori, Characterizing optical chirality, *Phys. Rev. A* **83**, 021803(R) (2011).
- [42] N. Mackinnon, On the differences between helicity and chirality, *J. Opt.* **21**, 125402 (2019).
- [43] D. L. Andrews, Quantum formulation for nanoscale optical and material chirality: Symmetry issues, space and time parity, and observables, *J. Opt.* **20**, 033003 (2018).
- [44] D. P. Craig and T. Thirunamachandran, *Molecular Quantum Electrodynamics: An Introduction to Radiation-Molecule Interactions* (Dover Publications, Mineola, NY, 1998).
- [45] M. Born and E. Wolf, *Principles of Optics: Electromagnetic Theory of Propagation, Interference and Diffraction of Light* (Elsevier, Amsterdam, 2013).
- [46] P. Woźniak, I. D. Leon, K. Höflich, G. Leuchs, and P. Banzer, Interaction of light carrying orbital angular momentum with a chiral dipolar scatterer, *Optica* **6**, 961 (2019).
- [47] K. A. Forbes and G. A. Jones, Measures of helicity and chirality of optical vortex beams, *J. Opt.* **23**, 115401 (2021).
- [48] K. A. Forbes and G. A. Jones, Optical vortex dichroism in chiral particles, *Phys. Rev. A* **103**, 053515 (2021).
- [49] R. M. Kerber, J. M. Fitzgerald, S. S. Oh, D. E. Reiter, and O. Hess, Orbital angular momentum dichroism in nanoantennas, *Commun. Phys.* **1**, 87 (2018).
- [50] Y. Iketaki, T. Watanabe, N. Bokor, and M. Fujii, Investigation of the center intensity of first- and second-order Laguerre-Gaussian beams with linear and circular polarization, *Opt. Lett.* **32**, 2357 (2007).
- [51] K. A. Forbes, Optical helicity of unpolarized light, *Phys. Rev. A* **105**, 023524 (2022).
- [52] D. Green and K. A. Forbes, Optical chirality of vortex beams at the nanoscale, *Nanoscale* **15**, 540 (2023).
- [53] K. A. Forbes and D. Green, Enantioselective optical gradient forces using 3D structured vortex light, *Opt. Commun.* **515**, 128197 (2022).
- [54] A. Forbes, Perspectives on the orbital angular momentum of light, *J. Opt.* **24**, 124005 (2022).
- [55] P. Shi, L. Du, and X. Yuan, Spin photonics: From transverse spin to photonic skyrmions, *Nanophotonics* **10**, 3927 (2021).
- [56] J. S. Eismann, L. H. Nicholls, D. J. Roth, M. A. Alonso, P. Banzer, F. J. Rodríguez-Fortuño, A. V. Zayats, F. Nori, and K. Y. Bliokh, Transverse spinning of unpolarized light, *Nat. Photonics* **15**, 156 (2021).
- [57] Y. Chen, F. Wang, Z. Dong, Y. Cai, A. Norrman, J. J. Gil, A. T. Friberg, and T. Setälä, Structure of transverse spin in focused random light, *Phys. Rev. A* **104**, 013516 (2021).
- [58] Z. Wang, C. Yan, F. Wang, Y. Chen, and Y. Cai, Effect of optical spatial coherence on localized spin angular momentum density in tightly focused light, *J. Opt. Soc. Am. A* **39**, C58 (2022).
- [59] Z. Wang, C. Yan, Z. Dong, F. Wang, Y. Chen, and Y. Cai, Effect of degree of polarization on localized spin density in tightly focusing of vortex beams, *IEEE Photonics J.* **14**, 1 (2022).
- [60] M. Hanifeh, M. Albooyeh, and F. Capolino, Optimally chiral light: Upper bound of helicity density of structured light for chirality detection of matter at nanoscale, *ACS Photonics* **7**, 2682 (2020).